

Cryogenic optical packaging of nanophotonic devices with coupling loss < 1 dB

BEIBEI ZENG^{1,§}, CHAWINA DE-EKNAMKUL^{1,§}, DANIEL ASSUMPCAO², DYLAN RENAUD², ZHUOXIAN WANG¹, DANIEL RIEDEL¹, JEONGHOON HA¹, CARSTEN ROBENS¹, DAVID LEVONIAN¹, MIKHAIL LUKIN³, MIHIR BHASKAR¹, DENIS SUKACHEV¹, MARKO LONCAR², BART MACHIELSE^{1,*}

¹AWS Center for Quantum Networking, Boston, MA 02135, USA

²John A. Paulson School of Engineering and Applied Sciences, Harvard University, Cambridge, MA 02138, USA

³Department of Physics, Harvard University, Cambridge, MA 02138, USA

[§]Equal contribution

*Corresponding author: machiel@amazon.com

A permanently packaged interface between a tapered optical fiber and nanophotonic devices is reproducibly demonstrated with a record-low coupling loss < 1 dB at ~730 nm that remains stable from 300 K to 30 mK.

Low-loss optical interfaces are crucial for optical information transport and processing across photonic and optoelectronic technologies. Efficient light transition between optical fibers and on-chip waveguides in photonic integrated circuits (PICs) has enabled numerous applications in optical/quantum interconnects [1, 2], optical switches, nonlinear optics, and quantum photonics [3, 4]. However, implementation of optical quantum computation [5] and communication [6, 7] platforms has been limited by the long-standing challenge of efficiently and reliably transferring photons into and out of quantum PICs at cryogenic temperatures, which are required to maintain high-fidelity quantum operations. Optical interfaces made of dissimilar materials experience thermal expansion mismatch as systems cool to the cryogenic temperatures, which imposes a fundamental tradeoff between coupling efficiency and stability. Recently, packaged optical interfaces with remarkable cryogenic stability have been demonstrated for nanophotonic devices without in-situ alignment [8-10]. Unfortunately, in these demonstrations coupling loss between optical fiber and nanophotonic devices is limited to roughly 10 dB [8] and 5 dB [9,10] at visible and telecom wavelengths, respectively, a level of loss which is prohibitive for many applications of quantum PICs.

Here we demonstrate highly efficient photonic packaging of the interface between a tapered optical fiber and diamond nanophotonic devices with a coupling loss of <1 dB per facet. The packaged nanophotonic device is cryogenically stable, surviving more than 5 thermal cycles down to 77 K with an efficiency change of less than 0.15 dB. It is also stable to sudden thermal shocks and

high-power laser illumination, enabling gas deposition based tuning and laser back-tuning of the resonance wavelength of the nanophotonic cavity inside in a dilution refrigerator [7]. It can be used for individual targeting of cavity resonances to quantum emitters, facilitating the operation of a nanocavity integrated quantum memory. We show that this technique is reproducible and compatible with multiple PIC platforms, including suspended diamond waveguides and thin film lithium niobate devices (SM).

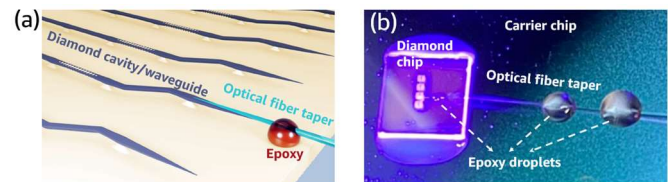


Fig. 1. (a) Illustration of the fiber-to-chip packaging concept. (b) The packaged device under UV illumination showing a series of epoxy droplets.

Fig. 1(a) shows the schematic of our packaging approach. For most of the demonstrations in this paper we choose as our target device a free-standing diamond waveguide optimized for efficient photon exchange with silicon vacancy color centers [7, 11]. The diamond device has a photonic crystal cavity which acts as a retroreflector away from its cavity resonance, and a tapered waveguide end used to create an adiabatic coupling interface with a tapered fiber [12, 13]. Once the fiber is coupled to the nanophotonic device; and verified using the measured reflection off the photonic crystal cavity, an epoxy droplet is placed a few hundreds of microns away from the waveguide-fiber interface to keep the tapers aligned. The epoxy is immediately UV cured to prevent flow and more epoxy droplets are placed further down the fiber to secure the pigtail shown in Fig. 1(b). We further UV cure the package for several hours to fully polymerize the epoxy. Once cured the sample can be

handled, transported, installed in vacuum chambers, and cooled down without specialized protection/treatment. The established procedure has successfully been utilized to reproduce 5 consecutive packaged devices with no failures, reaching coupling efficiencies limited primarily by diamond device properties [7, 8].

To test the cryogenic stability of the packaged devices, we place each fiber-packaged device in a liquid nitrogen flow cryostat. Because coefficients of thermal expansion scale with temperature, the majority of thermal contraction occurs between room temperature and 70 K [9,10]. This means that cooling to liquid nitrogen temperatures provides a reliable indicator of the device performance at sub-Kelvin temperatures. Fig. 2(a) shows the real-time coupling loss of a packaged device during one such thermal cycle. The laser is turned off during initial stage of cooldown to avoid optical tweezing of material outgassed from cryostat chamber. Once the laser is turned on, the reflected power remained steady at $\sim 83\%$ of the reference reflected power (SM). This includes two waveguide-fiber interfaces, reflection off the photonic crystal, and propagation through roughly 150 μm of diamond waveguide. We can thus establish a lower bound of one-way fiber-waveguide coupling efficiency of 91%, or equivalently coupling loss of 0.4 dB. A small gradual decrease in coupling efficiency is observed as a result of temperature-induced stress impacting polarization of transmitted light. This is corrected at low temperatures by optimizing the polarization of the input laser.

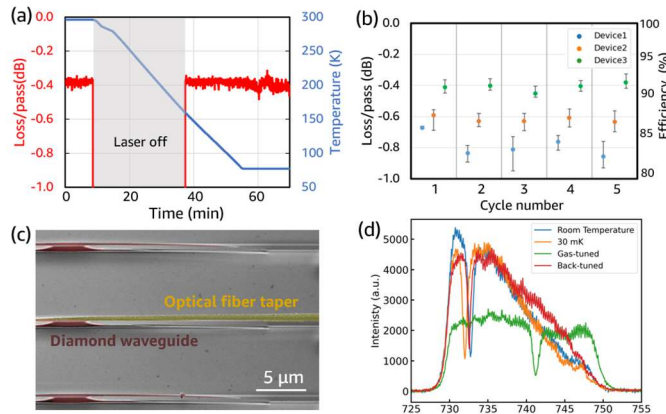


Fig. 2. (a) Measured loss and temperature as a function of time. (b) Statistics of 3 packaged devices over 5 thermal cycles. (c) SEM image of a packaged interface after 3 thermal cycles showing contact between tapered fiber and diamond waveguide. (d) Reflection spectra of the packaged diamond device at room temperature (blue), at 30 mK (orange), when gas-tuned (green), and back-tuned (red).

In Fig. 2(b), we document the average coupling loss at 77 K of 3 packaged devices as they passed through 5 thermal cycles. All samples show minimal performance degradation across five successive thermal cycles. The most heavily tested sample survived a total of more than 10 cycles without any observable changes in fiber alignment or coupling efficiency. Out of 5 tested samples, no failure was observed during thermal cycling. Fig. 2(c) shows a scanning electron microscope (SEM) image of a coupling interface after 3 successive thermal cycles. This confirms that the fiber taper remains firmly attached to the waveguide taper and the coupling interface is robust to the cryogenic environment.

We further demonstrate our technique's cryogenic compatibility and utility for quantum optics experiments by cooling a sample inside a dilution refrigerator and tuning the optical resonances of photonic crystal cavities by condensing nitrogen gas onto the sample surface. In Fig. 2(d), negligible degradation in coupling efficiency is observed as the device cools from room temperature to sub-Kelvin temperatures. Similarly, coupling efficiency remains steady as we carry out gas tuning by condensing nitrogen on the diamond surface tuning the cavity resonance by 10 nm. To tune the cavity resonance back, we send 60 μW of laser power to the device to induce local heating and evaporate deposited nitrogen, bringing the cavity back to within 1 nm of its original wavelength while preserving the coupling efficiency. Gas tuning and laser trimming provide a mechanism to dynamically tune cavity resonance wavelength to overcome any inhomogeneity between fabricated devices and target emitters. This experiment also demonstrates the packaged interface's robustness to mechanical, chemical, and temperature perturbations.

The cryogenically-compatible technique demonstrated here is material agnostic, and reproducibly enables permanently fiber-packaging of optical devices with small footprint, broad operational bandwidths, and high efficiency, lifting the limitations of photonic packaging in cryogenic environments. As a result, this technique provides an essential tool for improved performance and large-scale deployment of classical and quantum optical devices to a wide variety of challenging environments.

Acknowledgment We thank Nicholas Mondrik, Antia Lamas-Linares, Oskar Painter, Simone Severini, and Bill Vass for their operational support and technical guidance.

See Supplemental Material (SM) for supporting content.

REFERENCES

1. David A. B. Miller, Device requirements for optical interconnects to silicon chips, Proc. of the IEEE **97**, 1166 (2009).
2. David D. Awschalom et al., A Roadmap for Quantum Interconnects, Argonne National Laboratory (2022). <https://doi.org/10.2172/1900586>.
3. A. Sipahigil, et al. An integrated diamond nanophotonics platform for quantum-optical networks, Science **354**, 847 (2016).
4. A. W. Elshaari, W. Pernice, K. Srinivasan, O. Benson, and V. Zwiller, Hybrid integrated quantum photonic circuits, Nat. Photonics **14**, 285(2020).
5. F. Arute et al., Quantum supremacy using a programmable superconducting processor. Nature **574**, 505–510 (2019).
6. Nicolas Gisin, Rob Thew, Quantum communication, Nat. Photonics **1**, 165 (2007).
7. M. Bhaskar et al., Experimental demonstration of memory-enhanced quantum communication, Nature **580**, 60 (2020).
8. David J. Starling et al., A fully packaged multi-channel cryogenic module for optical quantum memories, [arXiv:2302.12919](https://arxiv.org/abs/2302.12919) (2023).
9. P. Timothy et al., Cryogenic packaging of an optomechanical crystal, Opt. Express **27**, 28782 (2019).
10. W. W. Wasserman et al., Cryogenic and hermetically sealed packaging of photonic chips for optomechanics, Opt. Express **30**, 30822 (2022).
11. P.-J. Stas et al., Robust multi-qubit quantum network node with integrated error detection, Science **378**, 557–560 (2022).
12. M. J. Burek et al., Fiber-Coupled Diamond Quantum Nanophotonic Interface, Phys. Rev. Applied **8**, 024026 (2017).
13. T. G. Tiecke et al., Efficient fiber-optical interface for nanophotonic devices, Optica **2**, 70 (2015).

CRYOGENIC OPTICAL PACKAGING OF NANOPHOTONIC DEVICES WITH COUPLING LOSS < 1 DB: SUPPLEMENTAL DOCUMENT

1. Tapered fiber fabrication

To prepare tapered optical fibers, we followed a wet etching procedure outlined in [1]. In this process, bare single-mode optical fibers (Thorlabs S630-HP) were etched in a hydrofluoric acid (HF) bath capped with a thin layer of o-xylene to promote taper formation at the acid-oil interface. Before immersion in HF, fibers are cleaned in a 200 °C sulfuric acid solution. To control the taper angle, fibers were drawn out of the etching solution at a constant rate. This speed, and the initial fiber diameter, determine the final taper length and angle. We tuned this parameter to obtain a taper angle of less than 4° to enable adiabatic mode transition from optical fiber to nanophotonic waveguides. We automate this procedure by motorizing the fiber movements between the different solutions, enabling mass production of tapered fibers. The fiber tapers can be further engineered by varying the speed of withdrawal from HF solution or by varying the temperature of the solution while the process is underway, enabling fine grained control of the fiber taper shape.

2. Diamond photonic crystal cavity

Diamond waveguide devices consist of a triangular cross-section nanobeam waveguide with a photonic crystal cavity and a tapered end. Devices were designed and fabricated using methods reported in [2, 3]. The waveguide and photonic crystal cavity were designed to support transverse electric (TE) guided and cavity modes at ~740 nm, respectively. Simulated photonic crystal reflection spectra (Lumerical FDTD) show a reflection coefficient of better than 96% across the wavelengths measured, thus contributing less than 0.15 dB to the reported loss figure.

3. Coupling efficiency measurement setup

Fig. S1 shows a fiber-based optical network used to measure the coupling loss/efficiency of the waveguide-fiber interface. We send 730 nm laser light from a laser diode (Thorlabs LP730-SF15) through a polarization controller into the fiber network. Light is split in a 99:1 fiber beam-splitter with 1% of the light sent to the device and 99% measured as reference power (A) using a photodiode. The reflected light from the device is then split in a 50:50 fiber beam-splitter sending 50% of the light to another photodiode (B). The other 50% of light can be sent to a spectrometer for simultaneous measurement of cavity spectrum and coupling efficiency when a broadband supercontinuum source is used.

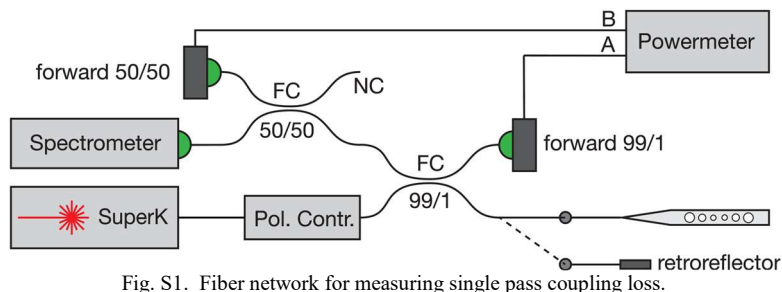


Fig. S1. Fiber network for measuring single pass coupling loss.

This technique enables accurate measurement of the reflection coefficient of the combined device and fiber interface while automatically compensating for fluctuations in the laser output power. The use of a single splice to connect the tapered fiber to the measurement setup introduces variation between packages of roughly 0.2 dB, thus driving the majority of the systematic variation between packages observed in our measurement.

4. Coupling efficiency simulations

In order to investigate the alignment tolerance, we simulate the coupling efficiency as a function of taper overlap, transverse shift and tilt of the fiber tip, respectively, using Lumerical MODE solutions, as shown in Fig. S2. The coupling loss between optical fiber and waveguide remains below 0.5 dB for a wide variety of alignment parameters. Changes in the overlap between the fiber and waveguide tapers from 60um to 20um (out of a total overlap distance of less than 60 um) results in a coupling change of only ~0.2 dB.

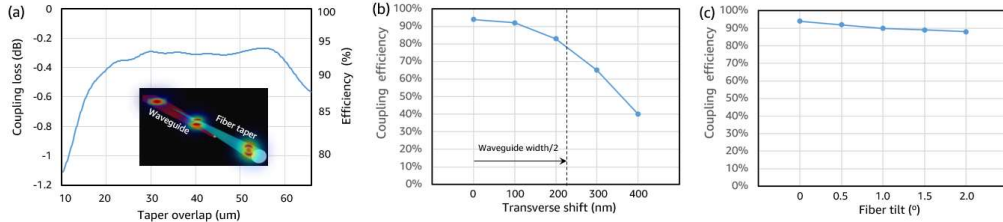


Fig. S2. Simulated coupling loss/efficiency as a function of the taper overlap (a) of an adiabatic interface between a tapered waveguide and fiber taper, (b) transverse offset, and (c) tilted angle of the fiber tip. Inset: Optical mode fields at different locations along the coupling interface.

The transverse offset only modestly impacts coupling efficiency/loss (~0.2 dB) when the misalignment is within ± 100 nm range of the ideal position, which can be achieved using commercially-available motorized translation stages. In addition, as long as tapered fiber tip is in contact with tapered waveguide and the titled angle is within ± 2 degrees, the coupling loss remains below -0.55 dB. The simulations show that the coupling is insensitive to a certain amount of misalignment, which agrees well with experimental observations. This waveguide-fiber interface is facilitated by strong van der Waals interactions, ensuring that once contact is made it can easily be maintained.

5. Alignment and assembly bench

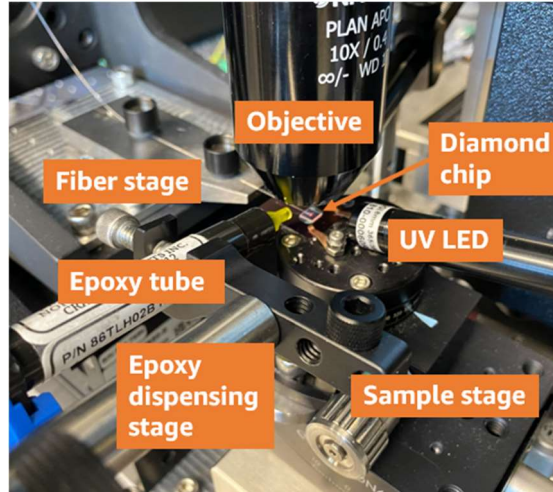


Fig. S3. Customized alignment and assembly bench for fiber manipulation and packaging.

The alignment and assembly bench shown in Fig. S3 consists of motorized translation and tilt stages for fiber alignment, an optical microscope for imaging, an optical coupling loss measurement system, an epoxy dispensing system, and a UV curing station. We first align the fiber to the device of interest and bring the tapers into contact (Fig. S4). Once coupled, the coupling is verified using measured reflection signal off the photonic crystal (Fig. S1). Then an

epoxy droplet is dispensed and cured a few hundreds of microns away from the waveguide-fiber interface to keep the tapers aligned. Finally, we secured the fiber pigtail by placing additional epoxy droplets further down the fiber.

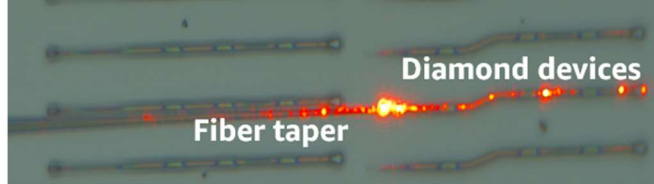


Fig. S4. Optical image of fiber-coupled diamond nanophotonic device.

This procedure has a number of advantages. First, the change in insertion loss is negligible before and after applying epoxy. This is because the epoxy droplet is far away from the point of contact and thus has a minimal impact on the coupling efficiency at the waveguide-fiber interface. As such coupling efficiency is limited by the efficiency of the waveguide-fiber interface, not the packaging process added afterwards. Second, this technique enables multiple fibers to be attached to a single chip, as there is minimal crosstalk between the attachment and curing of multiple interfaces. Finally, this approach does not require the use of valuable chip-edge space, as the fiber arrives at an angle and thus does not contact substrate at any point past the first epoxy droplet. This means that the chip edge real estate can be reserved for other optical and electronic interconnects and the density of interconnects on the chip can be increased.

6. Thermal cycling

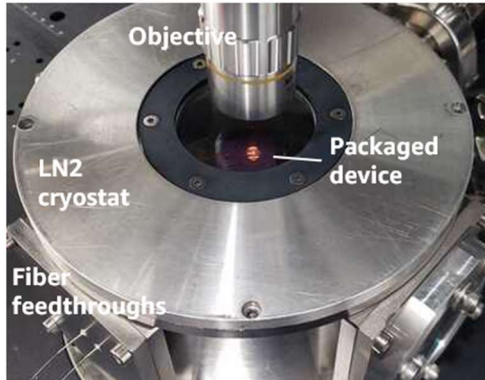


Fig. S5. Liquid nitrogen flow cryostat used for thermal cycling packaged samples down to 77K.

To test the cryogenic stability of our packaged devices, we place each packaged device in a liquid nitrogen (LN2) flow cryostat as shown in Fig. S5. Since the thermal contraction mainly occurs between room temperature and 70K [6], we monitor the coupling efficiency in real time by connecting a cryostat feedthrough fiber to the fiber network in Fig. S1. To start a thermal cycle, we mount the sample inside the sample chamber on a copper pedestal using a conductive silver paste to ensure thermalization. The sample chamber is pumped out with a turbo pump station to a base pressure of less than 10^{-4} mbar. Then we cool the sample at a rate of about 3-4 K per minute. To avoid optical tweezing of material freed from the cryochamber walls during cooldown, the laser is turned off until the temperature reaches 160K. At this temperature the laser is turned on and 20 μ W of power is sent to the waveguide and the intensity of the reflected light is monitored. We then keep the temperature constant at 77 K for an additional 30 minutes to allow the system to fully thermalize.

7. Packaging thin film lithium niobate (TFLN) devices

To demonstrate the compatibility of the packaging technique with other platforms, we test the procedure for packaging TFLN ridge waveguides. A narrowband retroreflector and a suspended tapered waveguide were etched into TFLN on oxide to enable testing of adiabatic fiber coupling/packaging. In simulation per facet loss was less than 0.5 dB — in line with simulations of loss for diamond waveguides coupled in the same manner. In practice measured reflectance was roughly -6 dB for two facets - leading to an upper bound of per facet loss of -3.2 dB. This efficiency was limited by the properties of the retroreflector and the associated couplers on the TFLN chip being tested, which could be further improved by engineering device geometries. But even at this level of loss, the technique (with a lower level of loss, a smaller footprint, and a wider coupling bandwidth) is competitive with the state-of-the-art grating couplers for TFLN devices, in which in-situ alignment is required at cryogenic temperatures.

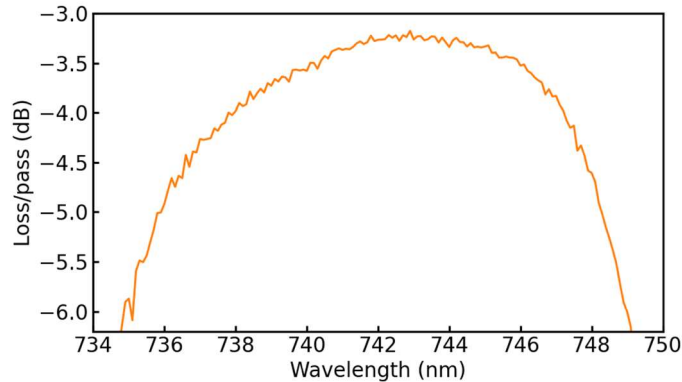


Fig. S6. Measured loss as a function of wavelength for TFLN devices.

Based on these results we believe this packaging technique could easily be adapted to operate with a wide variety of materials with low loss, and thus enable a variety of devices to be used in cryogenic, remote, or otherwise hostile environments.

8. Practical implementation for quantum memories

The packaging technique reported here will improve the performance and reduce the complexity of cryogenic quantum optics technologies, bringing them closer to deployment. In particular, packaging a tapered fiber to a device significantly reduces the complexity of cryogenic experiments used to operate diamond quantum network nodes [2] and state-of-the-art quantum transduction experiments [7]. As seen in Fig. S7 (a), using a packaged sample eliminates the need for a complex fiber coupling apparatus inside a dilution refrigerator. Specifically, this removes two sets of nanopositioning stages for fiber alignment, and the entire freespace imaging column from the system used to implement and image this alignment process. Removing these elements marks a significant step towards "plug-and-play" operation of quantum memories and enables the integration of multiple quantum memory devices inside a single cryogenic system, and thus their multiplexed utilization.

The multiplexing and high efficiency photon collection enabled by this technology will drive the performance of quantum repeater technology and photonic cluster state generation - key components of quantum communication and all optical quantum computation protocols. Fig. S7 (b) compares the performance of linear-optics measurement-device independent quantum key distribution (MDI-QKD) to upper-bounds for memory-enhanced MDI-QKD at different fiber-device coupling losses. Because the fidelity and rate of quantum communication drop at a superlinear rate as insertion loss increases [2] high efficiency photon collection plays a key part in the performance of quantum repeater protocols. Similar improvements are observed in cluster state formation where a single quantum emitter (coupled to a reservoir of

nearby memories) [5] serves as a mechanism for generating interactions between photons which arrive asynchronously at the optical device in Fig. S7 (c). As insertion loss decreases the maximum achievable cluster state size grows — making possible increasingly sophisticated quantum computation protocols. Here again the maximum number of detected photons grows exponentially with reductions in insertion loss.

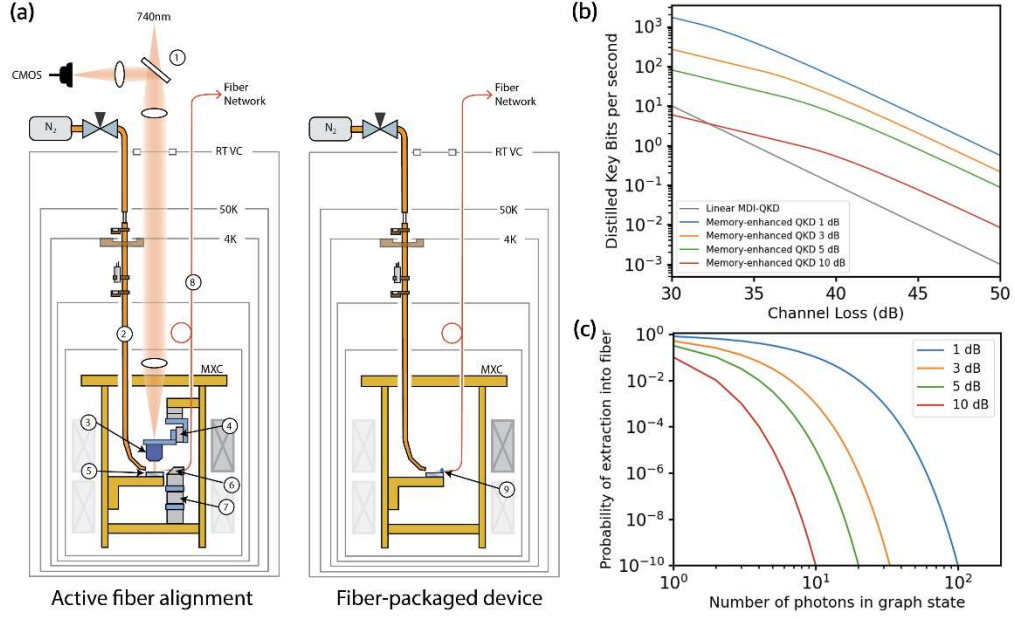


Fig. S7. (a) Footprint comparison of a gas-tuning experiment setup inside a dilution refrigerator with active fiber alignment apparatus versus fiber-packaging. 1: Freespace imaging column; 2: Gas tuning apparatus; 3: Objective; 4: Nanopositioners for objective; 5: Diamond chip containing waveguide devices; 6: Fiber mount; 16: Sample stage; 7: Nanopositioners for fiber; 8: Single-mode fiber S630-HP; 9: Fiber packaged device. (b) MDI-QKD communication rate using linear optics or memory enhanced quantum communication with device insertion loss limited by various efficiencies of optical fiber packaging. (c) Largest average cluster state that will be generated using quantum memories coupled to optical fiber with various levels of efficiency. Assumes a 10 MHz repetition rate for photon generation. In both (b) and (c) device performance scales superlinearly with reductions in insertion loss.

Memory-enhanced QKD of the kind demonstrated with SiVs [2] benefits heavily from a packaged fiber interface, which allows multiple quantum memories to be used on a single chip. Combined with wavelength division multiplexing, multiple quantum memories allow a linear scaling of qubit transmission rate. However, the performance of memory-enhanced MDI-QKD depends heavily on the efficiency of photon coupling from fiber to waveguide. The coupling efficiency affects the qubit rate both by adding additional effective loss to the incoming channels, but also, crucially, by determining what fraction of photons that have interacted with the memory arrive at the heralding detectors. Photons that interact with the memory but are lost before detection manifest as errors in the MDI-QKD scheme, which then require privacy amplification procedures to correct [4]. Privacy amplification reduces the fraction of arriving bits that can be used as key material.

To evaluate the performance of a QKD system using diamond nanophotonic cavities and glued fibers we calculate the effect of coupling efficiency η on the total key rate of a memory-enhanced MDI-QKD system in the style of [2]. We assume that the base fidelity of the memory system (from memory qubit errors and finite spin-photon fidelity) is 95% with additional infidelity added by the probability of a photon interacting with the memory but being lost before the detectors due to η :

$$QBER = QBER_{base} + p(\text{photon})(1 - \eta)$$

where N is the number of photon bins that are reflected from the memory during every attempt. We optimize N for every channel loss value to maximize the final key rate:

$$QKD\ Rate = r_s[Np(\text{photon})\eta]^2$$

where r_s is the fraction of raw bits remaining after privacy amplification. The results of this calculation are shown in Fig. S7(c).

Similarly, utilization of multi-photon quantum states for quantum information processing tasks such as one-way quantum communication and quantum computation require efficient optical coupling to quantum emitters [5]. For an N -photon state generated in a nanophotonic circuit, we can place an upper-bound on the probability of successfully coupling an N -photon state into a fiber of η^N , where $\eta = 1 - \text{loss}$ is the coupling efficiency from chip to fiber. Four example curves at 1, 3, 5, and 10 dB loss are plotted in Fig. S7(c), demonstrating the exponential decay in N -photon state detection probability as N increases. This illustrates the importance of chip-to-fiber coupling efficiency for experimentally generating, verifying, and utilizing photonic graph states for quantum information processing applications.

References

1. M. J. Burek et al., “Fiber-Coupled Diamond Quantum Nanophotonic Interface,” *Phys. Rev. Applied* **8**, 024026 (2017).
2. M. Bhaskar et al., “Experimental demonstration of memory-enhanced quantum communication,” *Nature* **580**, 60 (2020).
3. C. Chia et al., “Chapter Six - Diamond quantum nanophotonics and optomechanics,” *Semiconductors and Semimetals*, **104**, 219 (2021).
4. Nicolas Gisin, Grégoire Ribordy, Wolfgang Tittel, and Hugo Zbinden, “Quantum cryptography,” *Rev. Mod. Phys.* **74**, 145 (2022).
5. A. Vezvaei, P. Hilaire, M. F. Doty, and S. E. Economou, “Deterministic Generation of Entangled Photonic Cluster States from Quantum Dot Molecules,” *Phys. Rev. Applied* **18**, L061003 (2022).
6. W. Wang, H. Liu, R. Huang, Y. Zhao, C. Huang, S. Guo, Y. Shan, L. Li, “Thermal Expansion and Magnetostriction Measurements at Cryogenic Temperature Using the Strain Gauge Method,” *Front. Chem.* **6**, 72 (2018).
7. S Meesala et al. Non-classical microwave-optical photon pair generation with a chip-scale transducer <https://arxiv.org/abs/2303.17684>